THE JOURNAL OF BIOLOGICAL CHEMISTRY VOL. 286, NO. 49, pp. 42283–42291, December 9, 2011


# Size and Conformation Limits to Secretion of Disulfide-bonded Loops in Autotransporter Proteins*[S]

Received for publication, September 20, 2011, and in revised form, October 13, 2011 Published, JBC Papers in Press, October 17, 2011, DOI 10.1074/jbc.M111.306118

**Denisse L. Leyton[‡], Yanina R. Sevastsyanovich[‡], Douglas F. Browning[‡], Amanda E. Rossiter[‡], Timothy J. Wells[‡], Rebecca E. Fitzpatrick[‡], Michael Overduin[§], Adam F. Cunningham[‡], and Ian R. Henderson[‡1]**

*From the [‡]School of Immunity and Infection and the [§]School of Cancer Sciences, University of Birmingham, Birmingham B15 2TT, United Kingdom*

**Background:** There is a general paucity of cysteine residues within the passenger domains of autotransporter proteins.
**Results:** Distantly spaced cysteines forming disulfide-bonded loops or those enclosing structural elements are secretion-incompetent.
**Conclusion:** Only closely spaced cysteine pairs are compatible with the autotransporter pathway.
**Significance:** Secretion of folded peptides by the autotransporter pathway is limited; hence autotransporters lack large disulfide-bonded loops to remain secretion-competent.

**Autotransporters are a superfamily of virulence factors typified by a channel-forming C terminus that facilitates translocation of the functional N-terminal passenger domain across the outer membrane of Gram-negative bacteria. This final step in the secretion of autotransporters requires a translocation-competent conformation for the passenger domain that differs markedly from the structure of the fully folded secreted protein. The nature of the translocation-competent conformation remains controversial, in particular whether the passenger domain can adopt secondary structural motifs, such as disulfide-bonded segments, while maintaining a secretion-competent state. Here, we used the endogenous and closely spaced cysteine residues of the plasmid-encoded toxin (Pet) from enteroaggregative *Escherichia coli* to investigate the effect of disulfide bond-induced folding on translocation of an autotransporter passenger domain. We reveal that rigid structural elements within disulfide-bonded segments are resistant to autotransporter-mediated secretion. We define the size limit of disulfide-bonded segments tolerated by the autotransporter system demonstrating that, when present, cysteine pairs are intrinsically closely spaced to prevent congestion of the translocator pore by large disulfide-bonded regions. These latter data strongly support the hairpin mode of autotransporter biogenesis.**

Gram-negative bacteria possess seven secretion pathways (numbered I–VI and the chaperone-usher pathway) that facilitate navigation of secreted proteins through the inner membrane, periplasm, and outer membrane (OM).[2] These pathways generally use specialized machineries that span the width of the cell envelope and that differ in complexity, structural features, and mechanism of protein translocation. At first glance, the simplicity of the type Va secretion pathway appeared to be the exception; all the functional elements required for secretion appeared to be contained within a single protein with the N-terminal signal peptide mediating inner membrane translocation, the central passenger domain being the secreted functional moiety, and the C terminus forming a β-barrel structure in the OM, the latter element being essential for passenger domain translocation to the bacterial cell surface. Accordingly, the superfamily of proteins that exploit this pathway for their delivery to the surface of Gram-negative bacteria was termed autotransporters (ATs) (1).

However, recent studies demonstrating that passenger domain secretion requires the aid of accessory factors have challenged the theory that ATs are self-contained secretion systems; periplasmic chaperones SurA, Skp, and DegP have been implicated in AT biogenesis (2–5), as have BamA and BamD (5–8), the essential components of the OM β-barrel assembly machinery (BAM), which functions in concert to insert into the OM correctly folded integral outer membrane proteins (OMPs) that adopt a β-barrel conformation (9). Although it is clear that ATs associate closely and tightly with BamA and BamD during OM translocation (5, 10–12), the precise nature of these interactions is unknown. Certainly, it still remains to be elucidated how these components facilitate the integration of AT β-domains and other β-barrel OMPs into the lipid bilayer. Nevertheless, when inserted into the OM, the AT β-domain forms a β-barrel structure reminiscent of most other integral OMPs (13–18). Consistent with early bioinformatic studies, which suggested that the AT β-domain is evolutionarily and structurally conserved (19), almost perfectly superimposable crystal structures of the β-domain of five monomeric ATs have been reported (14–18). Each structure demonstrated a 12-stranded

* This work was supported by the Biotechnology and Biological Sciences Research Council (to M. O. and I. R. H.)
[S] The on-line version of this article (available at http://www.jbc.org) contains supplemental Tables S1–S3 and Figs. S1–S4.
[1] To whom correspondence should be addressed: Edgbaston, Birmingham B15 2TT, United Kingdom. Tel.: 44-121-414-4368; Fax: 44-121-414-3599; E-mail: i.r.henderson@bham.ac.uk.
[2] The abbreviations used are: OM, outer membrane; OMP, outer membrane protein; AT, autotransporter; BAM, β-barrel assembly machinery; Pet, plasmid-encoded toxin; D2A, domain-2A; β-ME, β-mercaptoethanol; Bis-Tris, 2-(bis(2-hydroxyethyl)amino)-2-(hydroxymethyl)propane-1,3-diol; TCEP, tris(2-carboxyethyl)phosphine; mPEG-Mal, mPEG-maleimide.

β-barrel adjoined by periplasmic turns and extracellular loops of varying length, with a narrow hydrophilic pore.

After insertion of the AT β-barrel into the OM, translocation through the β-barrel pore was thought to begin by the formation of a hairpin structure at the most C-terminal portion of the passenger domain, termed the autochaperone domain. There is now a substantial body of evidence demonstrating that the autochaperone domain emerges from the bacterial cell first and folds into a stable protease-resistant structure, which may drive folding of the remaining passenger domain and subsequent translocation across the OM in the absence of external energy sources (11, 20–23). OM translocation is dependent on a passenger domain conformation that differs from the final protein structure, which for most ATs is a characteristic right-handed β-helical stalk-like structure connected by various loops, some of which are presumed to confer functionality (21, 23–27).

The conformation of the passenger domain has important implications for secretion. Originally, it was hypothesized that the passenger domain was maintained in a linear state during secretion and that folding occurred only after translocation (1). However, other studies have challenged this model, suggesting that folded elements can readily be secreted to the bacterial surface (29, 30). Studies investigating this relationship between the folding and secretion of AT passenger domains have largely focused on disulfide bond formation during transit through the periplasm, between exogenous Cys residues introduced into passenger domains (20, 28), or between Cys residues within heterologous passenger domains (29–36). Although the translocation of sizable folded domains comprising disulfide-bonded segments of heterologous passenger domains was reported (30–32), a greater number of studies have demonstrated that periplasmic formation of either long disulfide-bonded loops or tightly folded/rigid structures is incompatible with OM translocation/secretion of AT passenger domains (20, 28, 29, 33–36). These dichotomous sets of studies have given rise to two mechanistic models of AT biogenesis, one proposing that passenger domain translocation occurs through a folded AT β-barrel pore, and the other proposing BamA as an accessory factor mediating passenger translocation before the β-domain adopts a final folded conformation.

Here, we used the plasmid-encoded toxin (Pet), a prototypical member of the serine protease ATs of the Enterobacteriaceae (SPATEs) (37), to ascertain the tolerance for folded elements during OM translocation. Pet possesses a pair of endogenous Cys residues separated by 4 amino acids that are located within a region of the passenger protein termed domain-2A (D2A), which is roughly 50 amino acids in length and is present only in the serine protease ATs of the Enterobacteriaceae that elicit toxic effects on eukaryotic cells (supplemental Fig. S1). We systematically determine the maximum length of a disulfide-bonded loop that does not interfere with translocation, providing data that strongly support the hairpin mode of AT biogenesis. In addition, we demonstrate that when present, native Cys pairs within AT passenger domains are intrinsically closely spaced to avoid jamming of the translocator pore by large disulfide-bonded regions.

## EXPERIMENTAL PROCEDURES

*Reagents, Media, and Bacterial Strains*—A polyclonal rabbit antiserum generated toward the Pet passenger domain (37) and BamA and BamD (8) have been previously described. Anti-FLAG tag antibody raised in rabbits and Alexa Fluor® 488 goat anti-rabbit IgG (H+L) were purchased from GenScript and Invitrogen, respectively. Anti-HA tag antibody produced in rabbits, alkaline phosphatase-conjugated goat anti-rabbit antibodies, and the alkaline phosphatase substrate 5-bromo-4-chloro-3-indolylphosphate were obtained from Sigma-Aldrich. Bacteria were grown at 37 °C in Luria-Bertani (LB) broth, and where necessary, the growth medium was supplemented with 100 μg/ml ampicillin, 50 μg/ml kanamycin, 2% D-glucose, or 0.02% L-arabinose. The *Escherichia coli* strains used in this study were TOP10 (Invitrogen) and BW25113 *dsbA*::*kan* (38).

*Plasmid Construction*—Plasmids used in this study are listed in supplemental Table S1. pBADPet has been described previously (39). A 363-bp SpeI-XbaI fragment comprising sequence coding for Pet without D2A was synthesized *de novo* and cloned into pUC57 (GenScript). pUC57ΔD2A was digested with SpeI and XbaI and subcloned into pBADPet, predigested with the same restriction enzymes, to create pBADPetΔD2A. To construct pUC57SB and pUC57L4HA, 624- and 771-bp fragments, respectively, were synthesized *de novo* and cloned into pUC57. pUC57SB and pUC57L4HA were digested separately with SalI and KpnI and with HpaI and EcoRI and subcloned into pBADPet, predigested with the same restriction enzymes, to create pBADPetSB and pBADPetL4HA, respectively. The Pet derivatives comprising one, two, and three HA epitope tags between the Cys pair in D2A were generated through *de novo* synthesis of 362-, 389-, and 416-bp SpeI-BsrGI fragments, respectively, that were then cloned into pUC57. pUC571HA, pUC572HA, and pUC573HA were digested with SpeI and BsrGI and subcloned into pBADPet, predigested with the same restriction enzymes, to create pBADPet1HA, pBADPet2HA, and pBADPet3HA, respectively. A 335-bp *de novo* synthesized fragment with Cys-12/Cys-17 mutated to Gly and His-1/Ser-50 mutated to Cys was cloned into pUC57 to create pUC5748aa. This vector was digested with SpeI and BsrGI and subcloned into pBADPet, predigested with the same restriction enzymes, to generate pBADPet48aa. The latter expresses a Pet derivative where the Cys residues are separated by 48 amino acids.

To construct pBADPetC12G, pBADPet6aa, pBADPet8aa, pBADPet10aa pBADPet12aa, pBADPet14aa, pBADPet16aa, and pBADPet9G, megaprimer PCR was performed as described previously (40) with some variation. Briefly, all round 1 PCRs were performed on 500 ng of template DNA (pBADPet) with 1 μg of the appropriate mutagenesis primer always in combination with 1 μg of primer BsrGIRv per 100 μl of reaction mixture. Round 1 PCRs were then purified to remove residual primers from the megaprimer synthesized in this first round of amplification. Round 2 PCRs were performed with 4 μg of megaprimer and 1 μg of primer SpeIFw on 500 ng of template DNA (pBADPet) per 100 μl of reaction mixture. Round 2 amplicons and target vector (pBADPet) were then digested with SpeI and BsrGI and ligated. Constructs pBADPetC12G/C17G, pBADPet18aa, and pBADPet20aa were generated

exactly as described above with the exception that pBADPetC12G was used as template DNA. The megaprimer PCR method was also used to generate pBADPet1HA-FLAG through insertion of a FLAG epitope tag between residues Gly-837 and Phe-838. Round 1 PCR was performed as described above using pBADPet as template DNA and the appropriate mutagenesis primer with primer SalIRv. Round 2 PCR ensued using primer BsrGIFw, and the subsequent amplicon and target vector (pBADPet) were then digested with BsrGI and SalI and ligated. pBADPet1HA-FLAG was digested with BsrGI and SalI and subcloned into pBADPetSB predigested with the same restriction enzymes to create pBADPetSB-FLAG. Primers used in this study are listed in supplemental Table S2.

*Construction of an E. coli TOP10 dsbA Mutant*—The λ Red recombinase system (41) was used to construct an in-frame *dsbA* knock-out mutant of *E. coli* TOP10.

*Analysis of Pet Biogenesis*—Growth, expression, and precipitation of Pet from TOP10 and TOP10 *dsbA*::*kan* transformed with pBADPet derivatives were performed as described previously (39). Where necessary, 10 mM β-mercaptoethanol (β-ME; Sigma-Aldrich) was added to the culture medium to reduce disulfide bonds formed in the periplasm (20). Supernatant proteins were separated by SDS-PAGE and detected by staining with Coomassie Brilliant Blue R250 (BDH Laboratory Supplies) or Western immunoblotting using anti-Pet passenger antibody.

*Immunofluorescence Microscopy*—Fixation and permeabilization of TOP10 cells transformed with pBADPet derivatives were performed as described previously (42). Preparation of cells for live cell imaging was performed as described previously (43) with minor modifications; poly-L-lysine-coated coverslips loaded with either fixed or live cells were washed three times with PBS, and nonspecific binding sites were blocked for 1 h in PBS containing 1% BSA (Europa Bioproducts). Coverslips were incubated with anti-Pet passenger, anti-HA tag, or anti-FLAG tag antibody for 1 h, washed three times with PBS, and incubated for an additional 1 h with Alexa Fluor® 488 goat anti-rabbit IgG. The coverslips were then washed three times with PBS, mounted onto glass slides, and visualized using either phase contrast or fluorescence using a Zeiss AxioImager Z2 microscope (100× objective) and an AxioCam MRm camera. Exposure time was 40 ms.

*Thiol Modifications*—Thiol modification reactions were performed to determine the presence or absence of disulfide bond formation in Pet using the thiol-specific reagent, mPEG-maleimide-10,000 Da (mPEG-Mal) (Sigma-Aldrich). Briefly, Pet from TOP10 cells transformed with pBADPet derivatives was expressed, and clarified supernatants were concentrated 100-fold as described previously (39). Supernatants were buffer-exchanged into thiol modification buffer (50 mM Tris, pH 7.5), and protein concentrations were calculated using Bradford protein assay reagent according to the manufacturer's instructions (Bio-Rad). mPEG-Mal was suspended in dimethyl sulfoxide (DMSO) as a 40 mM stock solution and used immediately. Briefly, 30 μg of protein, sometimes pretreated with 10 mM Tris(2-carboxyethyl) phosphine (Sigma-Aldrich) for 1 h at room temperature, was mixed with 10 mM mPEG-Mal in a final volume of 30 μl (topped up with thiol modification buffer where necessary) and incubated overnight at 4 °C. TCEP-treated (reduced) and untreated (oxidized) samples were mixed with the same volume of non-reducing SDS-sample buffer (2×), resolved on 4–20% gradient Precise protein gels in Tris-HEPES-SDS buffer (Thermo Fisher Scientific), and localized by Western immunoblotting using anti-Pet passenger antibody.

*Pet Purification and Circular Dichroism Spectroscopy*—TOP10 cells transformed with pBADPet and pBADPetΔD2A expressed Pet, and clarified supernatants were concentrated as described above. Pet and PetΔD2A were purified, and far-UV CD spectra were collected as described previously (21) except that Pet derivatives were purified using a HiLoad 16/60 Superdex 75 gel filtration column (GE Healthcare), and far-UV CD measurements were collected from 190 to 260 nm on a JASCO J-715 spectropolarimeter at room temperature with a 1-mm path length cell, 2-nm bandwidth, 1-nm increments, 2-s response, 100 nm/min scanning speed, and continuous scanning mode. Eight scans were averaged, and the spectrum was subtracted for buffer contribution.

*Co-immunoprecipitation*—Chemical cross-linking, spheroplast formation, and lysis of *E. coli* cultures for co-immunoprecipitation of BamA and BamD were performed as described previously (44). A total of 4 μg of anti-Pet passenger domain antibody was added into the cleared lysate, and the mixture was shaken for 1 h. A total of 60 μl of protein A-Sepharose beads (Sigma-Aldrich) was added to the lysate-antibody mixture, which was shaken for an additional 1 h. Beads within this mixture were pelleted (3,000 × *g*, 1 min) and washed three times with 1 ml of Pierce IP lysis buffer (Thermo Fisher Scientific) followed by one wash with 1 ml of PBS. Boiling in 50 μl of sample buffer containing DTT served to elute the proteins and to reverse the cross-linking reaction. The eluted fractions were centrifuged as above to completely remove the beads and separated on NuPAGE® 4–12% gradient Bis-Tris gels in MES buffer (Invitrogen). Western immunoblotting was carried out using rabbit polyclonal antibodies against the Pet passenger domain, BamA and BamD.

## RESULTS

*Native Cys Residues Are Not Required for Secretion or Folding of Pet*—With the exception of several polymorphic ATs of *Chlamydia* (45), a feature of AT proteins is the general paucity of Cys residues within the secreted passenger proteins. Where multiple Cys residues are present, the distances between the Cys pairs generally range from a minimum of 3 residues to a maximum of only 17 residues (46) (supplemental Table S3). It has previously been suggested that paired Cys residues found within AT passenger proteins are required for the correct biogenesis of ATs (46, 47). The Pet AT possesses a pair of endogenous Cys residues separated by 4 amino acids that are located within D2A. To determine the location of D2A, a three-dimensional model of Pet was built using the crystal structure of the homologous Hbp AT protein (26) (Fig. 1*A*). The model reveals that like Hbp, Pet possesses a serine protease domain (D1), which is N-proximal to the β-helix. In the case of Hbp, discursive loops extend from the central β-helix at different points to form D2 and D3 (25, 26). Both domains are lacking from Pet. However, Pet possesses D2A in place of D3, and the Pet amino

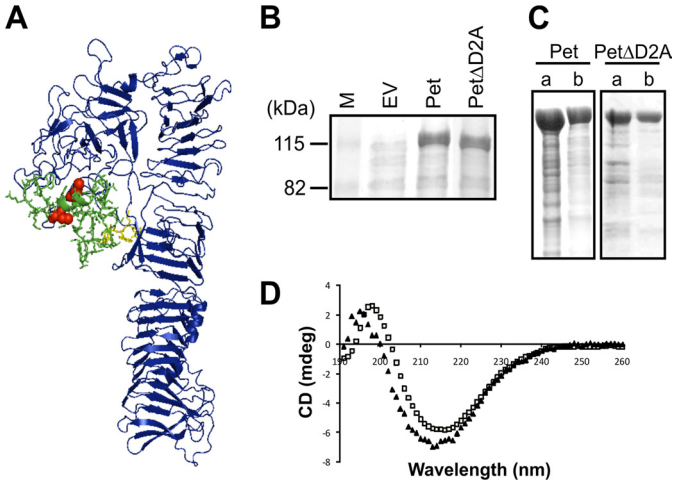


FIGURE 1. **The Cys residues and D2A are not required for secretion or folding of Pet.** *A*, a three-dimensional model of the Pet passenger domain showing D1 and the β-helix in *blue*, D2A in *green sticks*, the Cys pair in *red spheres*, and the semiconserved stable platform in *yellow sticks*. *B*, SDS-PAGE analysis of TCA-precipitated culture supernatant fractions harvested after growth of TOP10 expressing empty vector (*EV*), Pet, and PetΔD2A. *M*, molecular mass markers. *C*, SDS-PAGE analysis of concentrated supernatants from TOP10 expressing Pet and PetΔD2A before (*lane a*) and after (*lane b*) gel filtration chromatography. *D*, far-UV CD spectra of Pet (*open squares*) and PetΔD2A (*closed triangles*) in millidegrees (*mdeg*) showing maxima and minima at 199 and 217 nm and 196 and 214 nm, respectively.

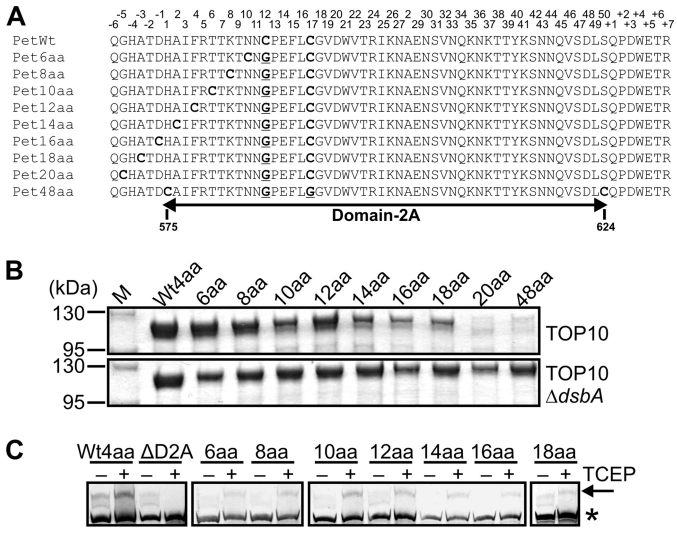


FIGURE 2. **Large disulfide-bonded regions abolish secretion of Pet.** *A*, alignment of D2A from Pet derivatives showing site-directed mutations that sequentially increased the distance between the endogenous Cys pair in D2A (*PetWt*) until OM translocation and secretion of the Pet passenger domain were stalled and abolished, respectively. Endogenous and exogenous Cys pairs are in *bold font*, and residues mutated to Gly are in *bold font* and *underlined*. Although D2A resides within residues 575–624 of the full-length protein, the *numbers* on top correspond to the position of each residue within D2A from His-1 to Ser-50. *B*, SDS-PAGE analysis of TCA-precipitated culture supernatant fractions harvested after growth of TOP10 (*top panel*) and TOP10 Δ*dsbA* (*bottom panel*) expressing wild-type Pet (*Wt4aa*) and Pet6aa to Pet48aa. *M*, molecular mass markers. *C*, mPEG-Mal labeling of wild-type Pet (*Wt4aa*), PetΔD2A, and Pet6aa to Pet48aa in the presence and absence of TCEP. Supernatants were harvested and concentrated after growth of TOP10 cells expressing wild-type Pet, PetΔD2A, and Pet6aa to Pet48aa. Samples were resolved on a gradient 4–20% Tris-HEPES-SDS-PAGE gel, and Pet was localized by Western immunoblotting using anti-Pet passenger antibody. The *arrow* indicates labeled/pegylated Pet, and the *asterisk* shows unlabeled/unpegylated Pet.

acid sequence directly adjacent to D2A (QPDWET) is almost completely conserved with Hbp (supplemental Fig. S1); it has been shown that these residues provide a platform for the projection of a stable external loop capable of independent movement (48). Thus, our model predicts that D2A contacts D1 and returns to the β-helical stem close to the point of departure such that the Cys residues do not form part of the central β-helical stem.

The model of the Pet passenger domain does not suggest an obvious reason why the Cys residues may influence passenger domain translocation. To determine whether the paired Cys residues or D2A were required for Pet biogenesis, culture supernatant fractions from *E. coli* cells expressing wild-type Pet (pBADPet) (39) and a D2A deletion construct (PetΔD2A; pBADPetΔD2A) were analyzed for the presence of proteins (Fig. 1*B*). SDS-PAGE demonstrated that Pet lacking D2A accumulated in the extracellular fraction at levels indistinguishable from wild-type Pet, indicating that D2A is not required for the expression, processing, or secretion of Pet. In addition, wild-type Pet and PetΔD2A were purified to >90% purity using gel filtration chromatography (Fig. 1*C*), and folding was monitored by far-UV CD spectroscopy. The far-UV CD spectra of both Pet and PetΔD2A are indicative of a folded structure rich in β-sheet, with characteristic maxima and minima between 195–200 nm and 210–220 nm, respectively (Fig. 1*D*). Although D2A appears not to be required for folding of the β-helix, PetΔD2A displayed a small blue shift in wavelength maxima and minima (−3 nm), conceivably reflecting a minor change in secondary structure in the D2A deletion mutant. To confirm that the Cys pair formed a disulfide bond, the mature secreted proteins were incubated with mPEG-Mal, in the presence or absence of TCEP, which specifically reduces disulfide bonds; mPEG-Mal interacts specifically with free thiol groups (Fig. 2*C*). Consistent with the lack of Cys residues, pegylation of PetΔD2A was not observed in the presence or absence of TCEP. In contrast, wild-type Pet was labeled with mPEG-Mal only under reduced conditions. Because faint high molecular weight bands were evident in both Pet and PetΔD2A under oxidizing conditions (−TCEP), they were therefore deemed nonspecific. These studies indicate that the paired Cys residues form disulfide bonds that are not required for the biogenesis of Pet.

*Large Disulfide-bonded Loops Abolish Secretion of Pet*—The nature of AT passenger domain translocation across the OM remains controversial. To address the conflicts arising from these datasets (20, 28–36) and to avoid artifacts that could result from heterologous constructs, we wished to address the issue of passenger domain translocation using an AT passenger domain that possesses endogenously paired Cys residues. The distances between endogenous Cys pairs in AT passenger domains generally range from a minimum of 3 residues to a maximum of only 17 residues (46) (supplemental Table S3). As such we hypothesized that Cys pairs separated by more amino acids would form disulfide-bonded loops in the periplasm that would block secretion. To test this hypothesis, we created pBADPet20aa and pBADPet48aa encoding mutant Pet proteins (Pet20aa and Pet48aa) in which the positions of the endogenous Cys residues within D2A of the Pet passenger domain were altered such that they were positioned 20 and 48 amino acids apart (Fig. 2*A* and supplemental Fig. S2). SDS-PAGE anal-

ysis of culture supernatant fractions derived from *E. coli* pBADPet20aa and pBADPet48aa revealed that Pet20aa and Pet48aa were not secreted into the culture medium (Fig. 2*B*, *top panel*). In contrast, when expressed in a strain lacking DsbA, stalling of passenger domain translocation across the OM was circumvented, and both proteins accumulated in the extracellular fraction (Fig. 2*B*, *bottom panel*). These results suggest that the 20 and 48 amino acids separating the Cys pairs in Pet20aa and Pet48aa, respectively, form disulfide-bonded loops that are too large to migrate through the diameter of the translocator pore, thereby stalling OM translocation and the subsequent secretion of the Pet passenger domain.

Having established that disulfide-bonded loops of 20 and 48 amino acids were incompatible with AT passenger domain translocation, we next set about determining the maximum number of endogenous residues that can form a disulfide-bonded loop that is tolerated by the translocator pore. We used site-directed mutagenesis to sequentially increase the distance between the Cys pair in D2A such that the Cys residues were separated by 6 (Pet6aa), 8 (Pet8aa), 10 (Pet10aa), 12 (Pet12aa), 14 (Pet14aa), 16 (Pet16aa), and 18 (Pet18aa) amino acids (Fig. 2*A* and supplemental Fig. S2). SDS-PAGE analyses of culture supernatant fractions from *E. coli* cells expressing Pet6aa to Pet18aa revealed that all mutant proteins could be secreted into the culture medium, albeit at reduced levels when compared with wild type for proteins containing larger disulfide-bonded loops (Fig. 2*B*, *top panel*). Furthermore, in the absence of DsbA, Pet14aa, Pet16aa, and Pet18aa accumulated in the extracellular compartment at levels resembling the wild-type protein. Pegylation experiments revealed that Pet6aa, Pet8aa, Pet10aa, Pet12aa, Pet14aa, Pet16aa, and Pet18aa interacted with mPEG-Mal only under reduced conditions (+TCEP), evidenced by a shift in the molecular weight of each protein (Fig. 2*C*), confirming the presence of a disulfide bond in the mature secreted species. Overall, our data demonstrate that the longest disulfide-bonded loop that does not significantly interfere with OM translocation of the Pet passenger domain is formed between a Cys pair separated by 18 residues.

*A Rigid Linker Interferes with OM Translocation*—Based on the data above, we hypothesized that the disulfide-bonded loops of stalled intermediates would be located in the periplasmic space. To address this hypothesis, we monitored disulfide bond-induced folding of the Pet passenger domain during transit through the periplasm when the distance between the endogenous Cys pair was increased via the insertion of one, two, or three HA epitope tags with the following amino acid sequence, YPYDVPDYA (Fig. 3*A*, *right panel*). Because the endogenous Cys pair within D2A of Pet is separated by 4 amino acids, the plasmids pBADPet1HA, pBADPet2HA, and pBADPet3HA encode Pet derivatives where the Cys pairs are separated by 13 (Pet1HA), 22 (Pet2HA), and 31 (Pet3HA) residues, respectively. We theorized that Pet1HA would be secreted but that Pet2HA and Pet3HA would form stalled intermediates. As expected, Pet2HA and Pet3HA did not accumulate in the culture supernatant fractions of *E. coli* pBADPet2HA or *E. coli* pBADPet3HA (Fig. 3*A*, *top* and *bottom panels*). However, surprisingly, Pet1HA was not secreted to the extracellular milieu from *E. coli* pBADPet1HA. In all three cases, stalling of

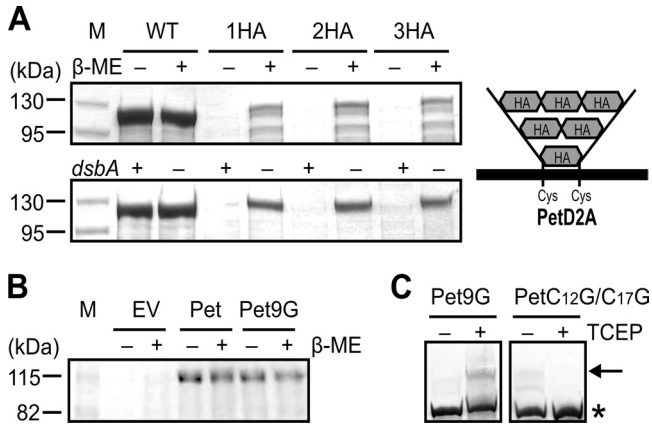


FIGURE 3. **A rigid linker interferes with OM translocation.** *A*, SDS-PAGE analysis of TCA-precipitated culture supernatant fractions harvested after growth of TOP10 and TOP10 Δ*dsbA* expressing Pet, Pet1HA (*1HA*), Pet2HA (*2HA*), and Pet3HA (*3HA*). Intramolecular disulfide bond formation was prevented through growth in the presence of β-ME (*top panel*) or in a *dsbA*$^-$ background (*bottom panel*). A schematic description of the HA epitope tag insertions is shown on the *right*. *M*, molecular mass markers. *B*, SDS-PAGE analysis of TCA-precipitated culture supernatant fractions harvested after growth of TOP10 expressing empty vector (*EV*), Pet, and Pet9G in the presence or absence of β-ME. *C*, mPEG-Mal labeling of Pet9G and PetC12G/C17G in the presence and absence of TCEP. Supernatants were harvested and concentrated after growth of TOP10 cells expressing Pet9G and PetC12G/C17G. Samples were resolved on a gradient 4–20% Tris-HEPES-SDS-PAGE gel, and Pet was localized by Western immunoblotting using anti-Pet passenger antibody. The *arrow* indicates labeled/pegylated Pet, and the *asterisk* shows unlabeled/unpegylated Pet.

passenger domain OM translocation could be circumvented under conditions preventing intramolecular disulfide bond formation through growth in the presence of reducing agent, β-ME (Fig. 3*A*, *top panel*), or in a *dsbA*$^-$ background (Fig. 3*A*, *bottom panel*). These latter data indicate that HA epitopes are not innately resistant to secretion via the AT translocator.

Our results were difficult to reconcile considering that the disulfide-bonded loop formed with one HA epitope tag was only 13 residues in length and that we had demonstrated the capacity of Pet to support the secretion of a passenger domain with a disulfide-bonded loop composed of 18 amino acids. Therefore, we decided to investigate whether it was the position, the nature, or the length of the HA epitope tag insertion that obstructed OM translocation of the Pet passenger domain by creating pBADPet9G, which codes for a Pet derivative (Pet9G) where the Cys pair is separated by 13 residues due to an insertion of 9 Gly residues. SDS-PAGE analysis of culture supernatant fractions from *E. coli* pBADPet9G revealed that Pet9G is expressed, processed, and secreted at wild-type levels in the presence or absence of β-ME (Fig. 3*B*). To determine whether secretion was unaffected because Pet9G failed to form a disulfide bond, Pet9G was isolated from the culture supernatants and subjected to pegylation using mPEG-Mal in the presence or absence of TCEP. As a control, we created pBADPetC12G/C17G, which codes for a Pet derivative where the endogenous Cys pair has been mutated to Gly. SDS-PAGE and Western immunoblotting of mPEG-Mal-treated samples revealed a shift in the molecular weight of Pet9G only under reduced conditions (+ TCEP; Fig. 3*C*). No such mobility shift was observed for PetC12G/C17G treated with TCEP, confirming that the Cys pair in Pet9G was disulfide-bonded. These data

indicate that when trapped within a disulfide-bonded loop, it is the rigid nature of the HA epitope that prevents secretion. Overall, our results indicate that both the nature and the length of the amino acid sequences contained between Cys residues are critical parameters for the translocation competence of passenger domains containing disulfide-bonded segments.

*Stalled Intermediates Possess a Hairpin Conformation*—Conceivably, OM translocation of Pet20aa, Pet48aa, Pet1HA, Pet2HA, and Pet3HA is initiated by the formation of a hairpin structure at the autochaperone domain and continues until the long disulfide-bonded loop or inflexible structure in D2A is reached, thereby jamming the translocator pore and preventing further transport of the passenger domain. Thus, it is conceivable that for Pet1HA, the disulfide-bonded loop containing the HA epitope is located in the periplasmic space when expressed in wild-type cells. Furthermore, we hypothesized that if a hairpin conformation was adopted, the C-terminal portion of the passenger domain would be exposed on the bacterial cell surface. To test these hypotheses, we generated pBADPet1HA-FLAG, a construct that encodes Pet1HA-FLAG, a Pet1HA derivative harboring a FLAG epitope tag (DYKDDDDK) in the C terminus of its passenger domain in addition to the HA epitope tag already present in D2A. The FLAG epitope tag was inserted between 2 residues (Gly-837 and Phe-838) that are present in a long loop projecting from the β-helix (supplemental Fig. S3*A*). Importantly, insertion of a FLAG epitope tag at this location did not abolish Pet secretion in a *dsbA*$^-$ background (supplemental Fig. S3*B*). As an additional control, pBADPetSB was created to encode PetSB, a Pet derivative containing mutations in the amino acid residues that are responsible for autocatalytic cleavage of the passenger domain from the translocator (Asn-1018 and Asp-1115); this secretion-blocked variant translocates the passenger domain to the cell surface, but it is not processed or released from the cell. A further derivative, PetSB-FLAG, was also constructed such that a FLAG epitope was positioned in the exact location as that in Pet1HA-FLAG.

To stain for surface exposure of the passenger domain, indirect immunofluorescence microscopy of live cells was used to reduce the possibility of cell lysis, and thus cells were expected to remain intact and impermeable toward antibodies (43). Fixed and permeabilized cells were used to stain for passenger exposure in the periplasm. We probed stalled intermediates with either anti-HA tag or anti-FLAG tag antibodies as well as anti-Pet passenger antibody as an additional control to demonstrate selective labeling of periplasmic and surface-exposed Pet passenger domain, respectively. As expected, live cells expressing Pet1HA and Pet1HA-FLAG did not label with anti-HA antibodies, and the HA epitope could be detected only if the cells were first permeabilized (Fig. 4, *middle panels*, compare *Pet1HA* and *Pet1HA (permeabilized)* with *Pet1HA-FLAG* and *Pet1HA-FLAG (permeabilized)*). These data indicate that the disulfide-bonded segment containing the HA epitope was localized in the periplasm and largely confirmed the preservation of OM integrity. As a positive control for anti-HA tag antibody labeling, we used PetL4HA, which has an HA epitope in extracellular L4 of the Pet β-barrel (Fig. 4, *middle panel*, *PetL4HA*). Labeling of Pet1HA and Pet1HA-FLAG with anti-Pet passenger antibody was suggestive of partial exposure of the passenger domain of these trapped intermediates at the cell surface and was comparable with that of the positive control, PetSB. Strong labeling of Pet1HA-FLAG with anti-FLAG tag antibody was also indicative of exposure of the C terminus of the passenger domain at the cell surface with labeling comparable with that of the positive control, PetSB-FLAG (Fig. 4, *right panels*, compare *Pet1HA-FLAG* with *PetSB-FLAG*). Collectively, these data demonstrate that Pet1HA and Pet1HA-FLAG are *bona fide* translocation intermediates that accumulate in the OM in a hairpin conformation with the N terminus exposed in the periplasm, whereas the C terminus of the passenger domain is exposed at the cell surface (supplemental Fig. S4).

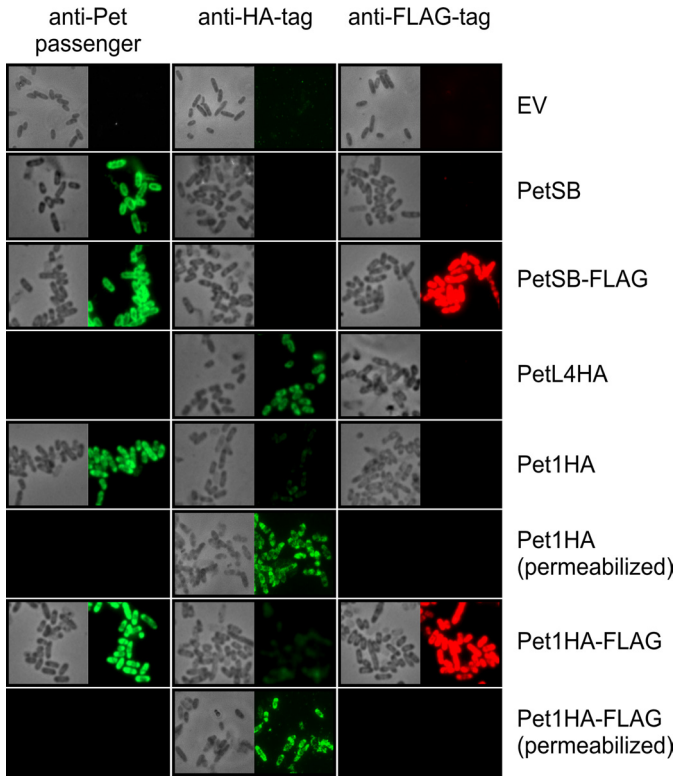


FIGURE 4. **Stalled intermediates possess a hairpin conformation that can be detected using fluorescence microscopy.** TOP10 cells expressing empty vector (*EV*), PetSB, PetSB-FLAG, PetL4HA, Pet1HA, and Pet1HA-FLAG were collected 1 h after induction with 0.02% arabinose and subjected to indirect immunofluorescence using anti-Pet passenger antibody (*left panels*), anti-HA antibody (*middle panels*), or anti-FLAG tag antibody (*right panels*; pseudo-colored *red*) and an Alexa Fluor 488-labeled conjugate (all panels). In the case of Pet1HA and Pet1HA-FLAG, half of the samples were fixed and permeabilized prior to labeling. Corresponding fields are also shown by phase contrast microscopy. *Completely black boxes* indicate that staining was not assessed.

*Stalled Intermediates Interact with BamA and BamD during OM Translocation*—We recently demonstrated that BamA and BamD are the only components of the BAM complex essential for AT biogenesis (8). This is further supported by *in vivo* cross-linking experiments documenting direct BamA/BamD-AT interactions (5, 10–12). Because AT secretion is extremely rapid (31), we performed co-immunoprecipitation assays via mild chemical cross-linking of proteins using formaldehyde to determine whether our stalled intermediates specifically interact with BamA and BamD *in vivo* during active translocation. Chemical cross-linking facilitates the identification of acces-

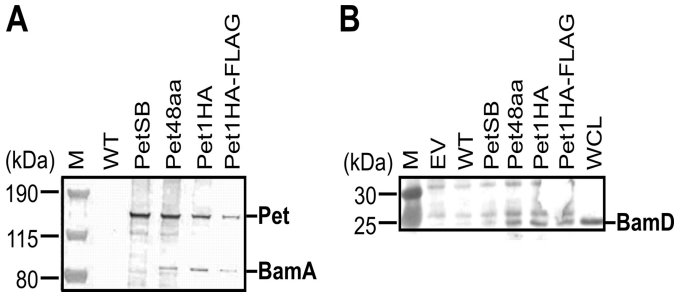


FIGURE 5. **Stalled intermediates interact with BamA and BamD during OM translocation.** TOP10 cells expressing empty vector (*EV*), wild-type Pet, PetSB, Pet48aa, Pet1HA, and Pet1HA-FLAG were harvested, spheroplasted, and lysed. Proteins were co-purified with anti-Pet passenger domain antibody, separated on a gradient 4–12% Bis-Tris gel in MES buffer, and analyzed by Western immunoblotting using anti-Pet passenger, anti-BamA (*A*), or anti-BamD (*B*) antibodies. A whole cell lysate (*WCL*) was included as an additional control for BamD. Generally, only the three high molecular weight stalled intermediates (Pet48aa, Pet1HA, and Pet1HA-FLAG) co-purify with the BAM proteins. *M*, molecular mass markers.

sory factors assisting in translocation of passenger domains across the OM (5, 22) and stabilizes these otherwise transient protein-protein interactions in whole cells. After cross-linking, *E. coli* cells expressing Pet48aa, Pet1HA, and Pet1HA-FLAG were harvested, spheroplasted, and lysed, and membrane proteins were co-purified with immobilized anti-Pet passenger domain antibody. Sample buffer containing DTT was used to elute stalled intermediates and interacting proteins and to dissociate the cross-linked proteins. Cells not expressing Pet or cells expressing wild-type Pet or the secretion-blocked variant (PetSB) were used as controls. Western immunoblotting using anti-Pet passenger, -BamA, or -BamD antibodies of eluates separated on gradient 4–12% Bis-Tris gels revealed that BamA specifically cross-links to and co-purifies with all three stalled intermediates that localized to the OM as high molecular mass intermediates of ~130 kDa and not with wild-type Pet or PetSB (Fig. 5*A*). These results exemplify the transient nature of the BamA-Pet interaction, which appears to transpire only during active translocation of the Pet passenger domain across the OM. In addition, all three stalled intermediates sequestered BamD, and this protein was also present in the eluates from cross-linked wild-type Pet and PetSB, albeit at considerably reduced levels (Fig. 5*B*).

## DISCUSSION

The dimensions of the translocator pore and the mechanism of OM translocation have direct implications for the degree of passenger domain folding prior to secretion. It is universally accepted that the fully folded AT $\beta$-domains, observed by x-ray crystallography, have pore diameters too narrow to accommodate significant structural elements within the passenger domains (14–18). However, translocation of sizable folded domains comprising disulfide-bonded segments of heterologous passenger domains has been reported (30–32). In contrast, most available evidence directly or indirectly indicates that OM translocation is dependent on a passenger domain conformation, which does not possess significant structural elements, is largely unfolded, and differs from the final protein structure (4, 11, 20, 21, 23, 49). The conflict between these data may arise through the use of non-native passenger domains and thus non-native structural elements. To address the dichotomous nature of these datasets, the secretion of an AT passenger domain that possesses a disulfide-bonded structural element formed by native Cys residues was examined.

We and others had previously noted the general paucity of Cys residues within the passenger domains of ATs (46). Here, updated bioinformatic analyses of the ATs confirmed that when present, Cys residues are juxtaposed with an average distance of ~7 residues and maximum distance of 17 residues (supplemental Table S3). The exceptions to this observation are the polymorphic ATs of *Chlamydia* (45). Interestingly, although *Chlamydia* do contain DsbA orthologues, which are expected to function to oxidize Cys-rich periplasmic proteins to form a substitute for peptidoglycan in the elementary body, the novel chlamydial periplasmic oxidoreductase, DsbH, may be responsible for maintaining a reducing periplasm (50). Although there is no direct evidence, it is tempting to speculate that DsbH keeps the polymorphic ATs of *Chlamydia* in a reduced state in the periplasm to maintain their translocation competence. These data strongly suggest that AT proteins have evolved to lack large disulfide-bonded loops within their passenger domains, but that they maintain the ability to secrete passenger domains with small disulfide-bonded structural elements. Certainly, the formation of small disulfide-bonded loops between closely spaced endogenous Cys residues does not to interfere with passenger domain translocation (24, 25, 31, 51).

To systematically determine the maximum length of a disulfide-bonded loop that does not interfere with passenger domain translocation, we analyzed the secretion of Pet. The Pet passenger domain possesses a pair of native Cys residues that form a disulfide bond, obviating the need for the introduction of heterologous domains that might obscure the data. Analysis of Pet and its single-site mutant derivatives demonstrates an apparent inverse relationship between the length of a disulfide-bonded loop and secretion efficiency and shows that the longest disulfide-bonded loop that does not significantly interfere with OM translocation of the Pet passenger domain is formed between a Cys pair separated by 18 residues. This is a distance that is in agreement with the preference for shorter connections in globular proteins where 49% of all disulfide bonds are formed between Cys pairs separated by less than 24 residues (52) and is not far removed from the maximum distance separating endogenous Cys pairs within some wild-type passenger domains. Thus, our results suggest that when present, Cys pairs are intrinsically closely spaced to prevent congestion of the translocator pore by large disulfide-bonded regions.

Having demonstrated that the AT $\beta$-domain is capable of secreting passenger domains with disulfide-bonded loops containing 18 amino acids, it was perplexing to find that a smaller loop containing an HA epitope tag insertion obstructed OM translocation of the Pet passenger. However, we demonstrated that it is the rigid and/or bulky nature rather than the position or length of the HA epitope tag insertion that is the critical parameter for translocation competence, indicating that only flexible regions with minimal tertiary structure are compatible with the AT pathway. This observation could explain the discrepancy in OM translocation efficiencies observed by others for disulfide-bonded heterologous passenger domains (29–36).

Indeed, our observations are consistent with the findings of Jong *et al.* (28), who showed that replacement of D2 with a 145-amino acid calmodulin moiety completely blocked the secretion of Hbp into the extracellular milieu when calcium was added to the growth medium to induce a conformational change in calmodulin in the form of a rigid dumbbell structure. The data are also consistent with observations by Rutherford *et al.* (53), who demonstrated that a folding-defective derivative of MalE could be translocated across the OM but that native MalE could not. These combined data strongly suggest the passenger must be maintained in a linear conformation with minimal structure to remain secretion-competent.

Based largely upon the contrasting observations for the secretion of disulfide-bonded segments, two prevailing models of passenger domain translocation have developed. The first encompasses translocation of a passenger domain through a folded AT β-domain pore via formation of a hairpin structure where a static strand is sequestered in the β-barrel lumen, whereas a sliding strand traverses the pore. Given the size constraints of the β-barrel pore, the passenger domain would have to be maintained in an extended conformation during the translocation event to prevent congestion. In this study, we determined the topology of *bona fide* translocation intermediates showing that they accumulate in the OM in a hairpin conformation with the N terminus of their passenger domains exposed in the periplasm, whereas their C terminus is exposed at the bacterial cell surface (supplemental Fig. S4). This result, in conjunction with the data demonstrating that secretion requires an unfolded passenger domain in a linear conformation, strongly supports the hairpin model of biogenesis.

The second model of passenger domain translocation suggests a role for BamA in maintaining an "open state" AT β-domain with complete folding occurring only after passenger domain translocation is complete; this model allows for the secretion of larger structural elements and glycosylated passenger domains. In support of this, several studies have demonstrated that BamA is essential for AT biogenesis (5–8). The interaction of our stalled intermediates with BamA *in vivo* during active translocation confirmed these observations. Recently, we demonstrated that BamD was also essential for passenger domain secretion, but that loss of the BamB, BamC, and BamE components had no effect on AT passenger secretion (8). The interaction of our stalled intermediates with BamD *in vivo* during active translocation confirmed these observations. Interestingly, interaction of BamD with the AT stalled intermediates was more prolonged than binding of BamA. These findings are consistent with a recent study demonstrating that the interaction of BamD with the AT β-domain persists after passenger domain translocation, cleavage, and secretion of the passenger (12). These authors also noted prolonged interaction of the AT β-barrel with BamB. However, BamB is not required for the insertion of Hbp or Pet β-barrels into the OM as folded species nor for translocation or folding of these passenger domains (5, 8). Furthermore, ATs are readily assembled in *Neisseria* sp., which lack BamB. Thus, we propose that the EspP-BamB and Hpb-BamB interactions observed *in vivo* (5, 10) are nonspecific and a consequence of BamB independently interacting with BamA.

The above data support a model in which the AT β-barrel docks with BamA and is maintained in an open and loosely folded conformation during passenger domain translocation with BamD required at a later step of AT biogenesis than BamA. Once the passenger domain is translocated, cleaved, and secreted, BamD would disassociate, triggering sealing of the AT β-domain and its folding into a stable barrel. This model conflicts with the simplistic hairpin model. The models may, however, be reconciled using recent observations for fimbrial biogenesis via the chaperone-usher pathway. Remarkably, Phan *et al.* (54) demonstrated that to allow translocation of the pilin subunit, the usher β-barrel rearranges from a kidney-shaped pore to a wider, near circular pore; such conformational contortions in β-barrel proteins were unprecedented as β-barrels were considered rigid structures. Notably, the AT barrel possesses a similar oval conformation to the usher; thus, we propose that the AT barrel adopts a circular conformation during passenger domain translocation, which allows migration of passenger domains with small disulfide-bonded segments and glycosyl moieties through the pore, and only after translocation and cleavage of the passenger domain are complete does the β-barrel "collapse" to the oval-shaped structure observed by crystallography. In this model, a stalled, trapped intermediate cannot shift to its final conformation and cannot be released from the BAM complex, a hypothesis consistent with the prolonged interactions observed between translocation-stalled intermediates and BamA and BamD.

*Acknowledgment—We thank Rosemary Parslow for access to the Birmingham Biophysical Characterization Facility.*

## REFERENCES


1. Pohlner, J., Halter, R., Beyreuther, K., and Meyer, T. F. (1987) *Nature* **325,** 458–462
2. Purdy, G. E., Fisher, C. R., and Payne, S. M. (2007) *J. Bacteriol.* **189,** 5566–5573
3. Wagner, J. K., Heindl, J. E., Gray, A. N., Jain, S., and Goldberg, M. B. (2009) *J. Bacteriol.* **191,** 815–821
4. Ruiz-Perez, F., Henderson, I. R., Leyton, D. L., Rossiter, A. E., Zhang, Y., and Nataro, J. P. (2009) *J. Bacteriol.* **191,** 6571–6583
5. Sauri, A., Soprova, Z., Wickström, D., de Gier, J. W., Van der Schors, R. C., Smit, A. B., Jong, W. S., and Luirink, J. (2009) *Microbiology* **155,** 3982–3991
6. Jain, S., and Goldberg, M. B. (2007) *J. Bacteriol.* **189,** 5393–5398
7. Voulhoux, R., Bos, M. P., Geurtsen, J., Mols, M., and Tommassen, J. (2003) *Science* **299,** 262–265
8. Rossiter, A. E., Leyton, D. L., Tveen-Jensen, K., Browning, D. F., Sevastsyanovich, Y., Knowles, T. J., Nichols, K. B., Cunningham, A. F., Overduin, M., Schembri, M. A., and Henderson, I. R. (2011) *J. Bacteriol.* **193,** 4250–4253
9. Knowles, T. J., Scott-Tucker, A., Overduin, M., and Henderson, I. R. (2009) *Nat. Rev. Microbiol.* **7,** 206–214
10. Ieva, R., and Bernstein, H. D. (2009) *Proc. Natl. Acad. Sci. U.S.A.* **106,** 19120–19125
11. Peterson, J. H., Tian, P., Ieva, R., Dautin, N., and Bernstein, H. D. (2010) *Proc. Natl. Acad. Sci. U.S.A.* **107,** 17739–17744
12. Ieva, R., Tian, P., Peterson, J. H., and Bernstein, H. D. (2011) *Proc. Natl. Acad. Sci. U.S.A.* **108,** E383–E391
13. Nikaido, H. (2003) *Microbiol. Mol. Biol. Rev.* **67,** 593–656
14. Barnard, T. J., Dautin, N., Lukacik, P., Bernstein, H. D., and Buchanan, S. K. (2007) *Nat. Struct. Mol. Biol.* **14,** 1214–1220
15. van den Berg, B. (2010) *J. Mol. Biol.* **396,** 627–633

16. Zhai, Y., Zhang, K., Huo, Y., Zhu, Y., Zhou, Q., Lu, J., Black, I., Pang, X., Roszak, A. W., Zhang, X., Isaacs, N. W., and Sun, F. (2011) *Biochem. J.* **435,** 577–587
17. Oomen, C. J., van Ulsen, P., van Gelder, P., Feijen, M., Tommassen, J., and Gros, P. (2004) *EMBO J.* **23,** 1257–1266
18. Tajima, N., Kawai, F., Park, S. Y., and Tame, J. R. (2010) *J. Mol. Biol.* **402,** 645–656
19. Loveless, B. J., and Saier, M. H., Jr. (1997) *Mol. Membr. Biol.* **14,** 113–123
20. Junker, M., Besingi, R. N., and Clark, P. L. (2009) *Mol. Microbiol.* **71,** 1323–1332
21. Renn, J. P., and Clark, P. L. (2008) *Biopolymers* **89,** 420–427
22. Soprova, Z., Sauri, A., van Ulsen, P., Tame, J. R., den Blaauwen, T., Jong, W. S., and Luirink, J. (2010) *J. Biol. Chem.* **285,** 38224–38233
23. Junker, M., Schuster, C. C., McDonnell, A. V., Sorg, K. A., Finn, M. C., Berger, B., and Clark, P. L. (2006) *Proc. Natl. Acad. Sci. U.S.A.* **103,** 4918–4923
24. Gangwer, K. A., Mushrush, D. J., Stauff, D. L., Spiller, B., McClain, M. S., Cover, T. L., and Lacy, D. B. (2007) *Proc. Natl. Acad. Sci. U.S.A.* **104,** 16293–16298
25. Johnson, T. A., Qiu, J., Plaut, A. G., and Holyoak, T. (2009) *J. Mol. Biol.* **389,** 559–574
26. Otto, B. R., Sijbrandi, R., Luirink, J., Oudega, B., Heddle, J. G., Mizutani, K., Park, S. Y., and Tame, J. R. (2005) *J. Biol. Chem.* **280,** 17339–17345
27. Emsley, P., Charles, I. G., Fairweather, N. F., and Isaacs, N. W. (1996) *Nature* **381,** 90–92
28. Jong, W. S., ten Hagen-Jongman, C. M., den Blaauwen, T., Slotboom, D. J., Tame, J. R., Wickström, D., de Gier, J. W., Otto, B. R., and Luirink, J. (2007) *Mol. Microbiol.* **63,** 1524–1536
29. Veiga, E., de Lorenzo, V., and Fernández, L. A. (1999) *Mol. Microbiol.* **33,** 1232–1243
30. Veiga, E., de Lorenzo, V., and Fernández, L. A. (2004) *Mol. Microbiol.* **52,** 1069–1080
31. Skillman, K. M., Barnard, T. J., Peterson, J. H., Ghirlando, R., and Bernstein, H. D. (2005) *Mol. Microbiol.* **58,** 945–958
32. Marín, E., Bodelón, G., and Fernández, L. Á. (2010) *J. Bacteriol.* **192,** 5588–5602
33. Klauser, T., Pohlner, J., and Meyer, T. F. (1990) *EMBO J.* **9,** 1991–1999
34. Klauser, T., Pohlner, J., and Meyer, T. F. (1992) *EMBO J.* **11,** 2327–2335
35. Jose, J., Krämer, J., Klauser, T., Pohlner, J., and Meyer, T. F. (1996) *Gene* **178,** 107–110
36. St Geme, J. W., 3rd, and Cutter, D. (2000) *J. Bacteriol.* **182,** 6005–6013
37. Eslava, C., Navarro-García, F., Czeczulin, J. R., Henderson, I. R., Cravioto, A., and Nataro, J. P. (1998) *Infect. Immun.* **66,** 3155–3163
38. Baba, T., Ara, T., Hasegawa, M., Takai, Y., Okumura, Y., Baba, M., Datsenko, K. A., Tomita, M., Wanner, B. L., and Mori, H. (2006) *Mol. Syst. Biol.* **2,** 2006.0008
39. Leyton, D. L., de Luna, M. G., Sevastsyanovich, Y. R., Tveen Jensen, K., Browning, D. F., Scott-Tucker, A., and Henderson, I. R. (2010) *FEMS Microbiol. Lett.* **311,** 133–139
40. Sarkar, G., and Sommer, S. S. (1990) *BioTechniques* **8,** 404–407
41. Datsenko, K. A., and Wanner, B. L. (2000) *Proc. Natl. Acad. Sci. U.S.A.* **97,** 6640–6645
42. Den Blaauwen, T., Aarsman, M. E., Vischer, N. O., and Nanninga, N. (2003) *Mol. Microbiol.* **47,** 539–547
43. Renn, J. P., and Clark, P. L. (2011) *Methods Enzymol.* **492,** 233–251
44. Diepold, A., Amstutz, M., Abel, S., Sorg, I., Jenal, U., and Cornelis, G. R. (2010) *EMBO J.* **29,** 1928–1940
45. Henderson, I. R., and Lam, A. C. (2001) *Trends Microbiol.* **9,** 573–578
46. Letley, D. P., Rhead, J. L., Bishop, K., and Atherton, J. C. (2006) *Microbiology* **152,** 1319–1325
47. Miyazaki, H., Yanagida, N., Horinouchi, S., and Beppu, T. (1989) *J. Bacteriol.* **171,** 6566–6572
48. Nishimura, K., Tajima, N., Yoon, Y. H., Park, S. Y., and Tame, J. R. (2010) *J. Mol. Med.* **88,** 451–458
49. Oliver, D. C., Huang, G., Nodel, E., Pleasance, S., and Fernandez, R. C. (2003) *Mol. Microbiol.* **47,** 1367–1383
50. Mac, T. T., von Hacht, A., Hung, K. C., Dutton, R. J., Boyd, D., Bardwell, J. C., and Ulmer, T. S. (2008) *J. Biol. Chem.* **283,** 824–832
51. Brandon, L. D., and Goldberg, M. B. (2001) *J. Bacteriol.* **183,** 951–958
52. Thornton, J. M. (1981) *J. Mol. Biol.* **151,** 261–287
53. Rutherford, N., Charbonneau, M. E., Berthiaume, F., Betton, J. M., and Mourez, M. (2006) *J. Bacteriol.* **188,** 4111–4116
54. Phan, G., Remaut, H., Wang, T., Allen, W. J., Pirker, K. F., Lebedev, A., Henderson, N. S., Geibel, S., Volkan, E., Yan, J., Kunze, M. B., Pinkner, J. S., Ford, B., Kay, C. W., Li, H., Hultgren, S. J., Thanassi, D. G., and Waksman, G. (2011) *Nature* **474,** 49–53

**Table S1. Plasmids used in this study**

| Plasmids | Relevant description | Reference |
|---|---|---|
| pUC57 | Cloning vector, ampicillin resistant | GenScript |
| pUC57SB | pUC57 derivative containing a *de novo* synthesized *SB Sal*I-*Kpn*I fragment | GenScript / This study |
| pUC57ΔD2A | pUC57 derivative containing a *de novo* synthesized Δ*D2A Spe*I-*Xba*I fragment | GenScript / This study |
| pUC571HA | pUC57 derivative containing a *de novo* synthesized *D2A1HA* epitope *Spe*I-*BsrG*I fragment | GenScript / This study |
| pUC572HA | pUC57 derivative containing a *de novo* synthesized *D2A2HA* epitope *Spe*I-*BsrG*I fragment | GenScript / This study |
| pUC573HA | pUC57 derivative containing a *de novo* synthesized *D2A3HA* epitope *Spe*I-*BsrG*I fragment | GenScript / This study |
| pUC5748aa | pUC57 derivative containing a *de novo* synthesized *D2A48aa Spe*I-*BsrG*I fragment | GenScript / This study |
| pUC57L4HA | pUC57 derivative containing a *de novo* synthesized *L4HA Hpa*I-*Eco*RI fragment | GenScript / This study |
| pBADHisA | Arabinose-inducible expression vector, ampicillin resistant | Invitrogen |
| pBADPet | pBADHisA derivative expressing *de novo* synthesized Pet | (39) |
| pBADPetSB | pBADPet derivative containing a *Sal*I-*Kpn*I fragment subcloned from pUC57SB where putative autocatalytic residues N1018 and D1115 were mutated to Gly to create a secretion blocked variant | This study |
| pBADPetΔD2A | pBADPet derivative containing a *Spe*I-*Xba*I fragment subcloned from pUC57ΔD2A that contains three Gly residues between $H_1$ and $S_{50}$ to express Pet with a D2A deletion | This study |
| pBADPet1HA | pBADPet derivative containing a *Spe*I-*BsrG*I fragment subcloned from pUC571HA to express Pet with one HA epitope between residues $E_{14}$ and $F_{15}$ | This study |
| pBADPet2HA | pBADPet derivative containing a *Spe*I-*BsrG*I fragment subcloned from pUC572HA to express Pet with two HA epitopes between residues $E_{14}$ and $F_{15}$ | This study |
| pBADPet3HA | pBADPet derivative containing a *Spe*I-*BsrG*I fragment subcloned from pUC573HA to express Pet with three HA epitopes between residues $E_{14}$ and $F_{15}$ | This study |
| pBADPet$C_{12}$G | pBADPet derivative with $C_{12}$ mutated to Gly to disturb the Cys pair within Pet and obstruct disulfide bond formation | This study |
| pBADPet$C_{12}$G/ $C_{17}$G | pBADPet derivative with $C_{12}$ and $C_{17}$ mutated to Gly to disturb the Cys pair within Pet and obstruct disulfide bond formation | This study |
| pBADPet6aa | pBADPet derivative with $N_{10}$ mutated to C and $C_{12}$ to G so that the Cys pair in Pet are separated by 6 amino acids | This study |
| pBADPet8aa | pBADPet derivative with $K_8$ mutated to C and $C_{12}$ to G so that the Cys pair in Pet are separated by 8 amino acids | This study |
| pBADPet10aa | pBADPet derivative with $T_6$ mutated to C and $C_{12}$ to G so that the Cys pair in Pet are separated by 10 amino acids | This study |
| pBADPet12aa | pBADPet derivative with $F_4$ mutated to C and $C_{12}$ to G so that the Cys pair in Pet are separated by 12 amino acids | This study |
| pBADPet14aa | pBADPet derivative with $A_2$ mutated to C and $C_{12}$ to G so that the Cys pair in Pet are separated by 14 amino acids | This study |
| pBADPet16aa | pBADPet derivative with $D_{-1}$ mutated to C and $C_{12}$ to G so that the Cys pair in Pet are separated by 16 amino acids | This study |

| | | |
|---|---|---|
| pBADPet18aa | pBADPet derivative with $A_{-3}$ mutated to C and $C_{12}$ to G so that the Cys pair in Pet are separated by 18 amino acids | This study |
| pBADPet20aa | pBADPet derivative with $G_{-5}$ mutated to C and $C_{12}$ to G so that the Cys pair in Pet are separated by 20 amino acids | This study |
| pBADPet48aa | pBADPet derivative containing a *Spe*I-*BsrG*I fragment subcloned from pUC5748aa containing $C_{12}$/$C_{17}$ mutated to G and $H_1$/$S_{50}$ to C so that the Cys pair in Pet are separated by 48 amino acids | This study |
| pBADPet9G | pBADPet derivative with a nine 9 amino acid Gly linker inserted in Pet between $E_{14}$ and $F_{15}$ | This study |
| pBADPet1HA-FLAG | pBADPet1HA derivative with one FLAG epitope inserted in Pet between residues G837 and F838 | This study |
| pBADPetSB-FLAG | pBADPetSB derivative with one FLAG epitope inserted in Pet between residues G837 and F838 | This study |
| pBADPetL4HA | pBADPet derivative containing a *Hpa*I-*Eco*RI fragment subcloned from pUC57L4HA with one HA epitope inserted in loop 4 of the Pet β-barrel between residues G1184 and M1185 | This study |

Note that the numbers next to the Cys residues correspond to their position relative to D2A (from $H_1$ to $S_{50}$) and not the full length protein (from H575 to S624).

**Table S2. Primers used in this study**

| Primer | Sequence | Reference |
|---|---|---|
| *Spe*IFw | 5'-CC**ACTAGT**TATGCAGGGTCACGCGACCG-3' | This study |
| *BsrG*IRv | 5'-GC**TGTACA**GGTCGATGTACGCGGTTTTG-3' | This study |
| *BsrG*IFw | 5'-CC**TGTACA**GCGGTAAAAACATCACCGGC-3' | This study |
| *Sal*IRv | 5'-TGAA**GTCGAC**CAGCAGCAGGTTGTTCGC-3' | This study |
| $MPN_{10}C/C_{12}G$(6-aa) | 5'-GCGATCTTCCGTACCACCAAAACCTGCAACGGTCCGGAATTTCTGTGCGGTGTTG-3' | This study |
| $MPK_8C/C_{12}G$(8-aa) | 5'-CCACGCGATCTTCCGTACCACCTGCACCAACAACGGTCCGGAATTTCTGTGCGGTGTTG-3' | This study |
| $MPT_6C/C_{12}G$(10-aa) | 5'-GACCGACCACGCGATCTTCCGTTGCACCAAAACCAACAACGGTCCGGAATTTCTGTGCGGTGTTG-3' | This study |
| $MPF_4C/C_{12}G$(12-aa) | 5'-GTCACGCGACCGACCACGCGATCTGCCGTACCACCAAAACCAACAACGGTCCGGAATTTCTGTGCGGTGTTG-3' | This study |
| $MPA_2C/C_{12}G$(14-aa) | 5'-GCAGGGTCACGCGACCGACCACTGCATCTTCCGTACCACCAAAACCAACAACGGTCCGGAATTTCTGTGCGGTGTTG-3' | This study |
| $MPD_{-1}C/C_{12}G$(16-aa) | 5'-GTTATGCAGGGTCACGCGACCTGCCACGCGATCTTCCGTACCACCAAAACCAACAACGGTCCGGAATTTCTGTGCGGTGTTG-3' | This study |
| $MPA_{-3}C$ (18-aa) | 5'-GCGCCACTAGTTATGCAGGGTCACTGCACCGACCACGCGATCTTCCGTACC-3' | This study |
| $MPG_{-5}C$ (20-aa) | 5'-CAAAAACGCGCCACTAGTTATGCAGTGCCACGCGACCGACCACGCGATCTTCC-3' | This study |
| $MPC_{12}G$ | 5'-CTTCCGTACCACCAAAACCAACAACGGTCCGGAATTTCTGTGCGGTGTTGAC-3' | This study |
| $MPC_{17}G$ | 5'-CCAACAACGGTCCGGAATTTCTGGGCGGTGTTGACTGGGTTACCCGTATC-3' | |
| MP9G | 5'-CCACCAAAACCAACAACTGCCCGGAA*GGTGGCGGTGGCGGTGGCGGTGGCGGT*TTTCTGTGCGGTGTTGACTGGGTTAC-3' | This study |
| MP1HA-FLAG | 5'-CGCTGGCGATGCTGGACGGT*GATTATAAAGATGATGATGATAAA*TTCGACACCTCTTACCAGGG-3' | This study |

Restriction enzyme sequences are in bold font, site-directed mutations are underlined and insertion sequences are italicized. Note that the numbers next to the Cys residues correspond to their position relative to D2A (from $H_1$ to $S_{50}$) and not the full length protein (from H575 to S624).

**Table S3. Cys pairs within passenger domains of selected ATs**

| Protein | Organism | Function | No. of Cys | Distance between Cys pairs | Accession no. |
|---|---|---|---|---|---|
| **SPATEs** | | | | | |
| EspC | *E. coli* | Toxin | 3 | 13/6 | AAC44731 |
| EspP | *E. coli* | Toxin | 2 | 9 | CAA66144 |
| Pet | *E. coli* | Toxin | 2 | 4 | AAC26634 |
| Sat | *E. coli* | Toxin | 2 | 5 | AAG30168 |
| SigA | *S. flexneri* | Toxin | 2 | 5 | AAF67320 |
| RpeA | *E. coli* | Colonization factor | 2 | 10 | AAT36311 |
| Vat | *E. coli* | Toxin | 2 | 11 | AAO21903 |
| **Non-SPATEs** | | | | | |
| AlpA | *H. pylori* | Adhesion | 2 | 16 | CAB05386 |
| AlpB | *H. pylori* | Adhesion | 2 | 17 | BAJ59997 |
| ApeE | *S. enterica* | Esterase | 2 | 8 | AAC38796 |
| App | *N. meningitidis* | Adhesion | 2 | 10 | CAC14670 |
| AusI/MspA | *N. meningitidis* | Adhesion | 4 | 10/9 | ABB99955/ NP_274990 |
| AutA | *N. meningitidis* | Unknown | 2 | 4 | CAB89117 |
| EstA | *P. aeruginosa* | Cell mobility, biofilm formation, esterase | 2 | 5 | AAB61674 |
| Hap | *H. influenzae* | Adhesion | 2 | 10 | P45387 |
| IcsA | *S. flexneri* | Intracellular movement | 3 | 3 | AAA26547 |
| IgA1 | *H. influenzae* | Protease | 2 | 10 | P45386 |
| IgA1 | *N. gonorrhoeae* | Protease | 2 | 10 | P09790 |
| IgA1 | *N. meningitidis* | Protease | 2 | 10 | CAA57857 |
| Lip-1 | *X. luminescens* | Lipase | 2 | 8 | P40601 |
| McaP | *M. catarrhalis* | Adhesion, lipase, esterase | 2 | 11 | AAP97134 |
| NalP | *N. meningitidis* | Cleavage of ATs | 4 | 6/6 | AAN71715 |
| PmpD | *C. trachomatis* | Adhesion | 24 | NA | O84818 |
| Pmp20 | *C. pneumoniae* | Adhesion | 14 | NA | Q9Z812 |
| PspA | *P. fluorescens* | Unknown | 2 | 6 | BAA36466 |
| PspB | *P. fluorescens* | Unknown | 4 | 6/4 | BAA36467 |
| SabA | *H. pylori* | Adhesion | 4 | 5/4 | AAD06240 |
| SphB1 | *B. pertussis* | Cleavage of FHA | 2 | 6 | AJ318229 |
| Ssa1 | *P. haemolytica* | Unknown | 2 | 6 | AAA80490 |
| Ssp | *S. marcescens* | Protease | 4 | 6/4 | P09489 |
| Ssp-h1 | *S. marcescens* | Unknown | 4 | 6/4 | BAA33455 |
| Ssp-h2 | *S. marcescens* | Unknown | 4 | 6/4 | BAA11383 |
| VacA | *H. pylori* | Toxin | 2 | 10 | Q48247 |

FHA, filamentous hemagglutinin, a two-partner secretion protein from *B. pertussis*; NA, not assessed.

**Supplementary Figure Legends**

**Fig. S1.** Alignment demonstrating that D2A (shown in bold font) and the conserved Cys residues (shown in bold font and underlined) are present only in cytotoxic SPATE proteins. The conserved stable platform present in all SPATE proteins is underlined. Note that numbers correspond to the position of D2A relative to the full length protein (from H575 to S624).

**Fig. S2.** A three-dimensional model of the Pet passenger domain showing D1 and the β-helix in blue, D2A in green and boxed with solid lines, the Cys pair in red spheres, and the semi-conserved stable platform in yellow sticks and boxed with broken lines. The positions of the Cys pair in Pet6aa to Pet48aa are also shown.

**Fig. S3.** A FLAG epitope tag in the C-terminus of the Pet passenger domain does not abolish secretion. (A) A three-dimensional model of the Pet passenger domain showing a FLAG epitope tag (yellow spheres) inserted between two residues (G837 and F838) that are present in a long loop projecting from the β-helix. (B) SDS-PAGE analysis of TCA-precipitated culture supernatant fractions harvested after growth of TOP10 *ΔdsbA* expressing wild-type Pet (WtPet) and Pet1HA-FLAG. M; molecular weight markers.

**Fig. S4.** A schematic description of stalled versus secreted passenger domains. In an oxidizing environment (wild-type cells; left), OM translocation of Pet1HA-FLAG is initiated by the formation of a hairpin structure and continues until the inflexible HA epitope (green rectangle) in D2A is reached thereby jamming the translocator pore and preventing further transport of the passenger domain. As such, intermediates accumulate in the OM in a hairpin conformation with the N-terminus (containing the HA epitope) exposed in the periplasm while the C-terminus of the passenger domain [containing the FLAG epitope (red box)] is exposed at the cell surface. In a reducing environment (Δ*dsbA* cells; right), OM translocation is unaffected as the HA epitope is not trapped within a disulfide-bonded loop and is not innately resistant to secretion via the AT translocator. Once on the bacterial cell surface, the protein folds into its native conformation, is processed and secreted into the extracellular environment.

Fig. S1


Toxic SPATEs
Non-toxic SPATEs
Pet QGHATDHAIFRTTKTNNCP-----EFLCGVDWVTRIKNAENSVNQKNKTTYKSNNQVSDLSQPDWETR
Sat QGHATEHAIFRSS-ANHCSL----VFLCGTDWVTVLKETESSYNKKFNSDYKSNNQQTSFDQPDWKTG
EspP QGHATEHAIYRDG-AFSCSLPAPMRFLCGSDYVAGMQNTEADAVKQNGNAYKTNNAVSDLSQPDWETG
SigA QGHATEHAIFKEG-NNNCPIP----FLCQKDYSAAIKDQESTVNKRYNTEYKSNNQIASFSQPDWESR
EspC AGTCLHLMLFLERVGVTCMLP---GVICEKDYVSGIQQQENSANKNNNTDYKTNNQVSSFEQPDWENR
Tsh QGHPVIHAYNTQSVADKLAAS----------GDHSVLTQPTSFSQEDWENR
Hbp QGHPVIHAYNTQSVADKLAAS----------GDHSVLTQPTSFSQEDWENR
Vat QGHPVIHASTSQSIANTVSSL----------GDNSVLTQPTSFTQDDWENR
Pic QGHPVIHASISG----------SAPVSLNQKDWENR
SepA QGHPVIHAG----------TTTSSSQSDWETR
EatA QGHPVIHAG----------MTTSAGQSDWENR
EpeA QGHPVIHA----------GVGVSAEQNDWETR
EspI QGHPVIHA----------GQTVSASQSDWENR
575
624

**Fig. S2**

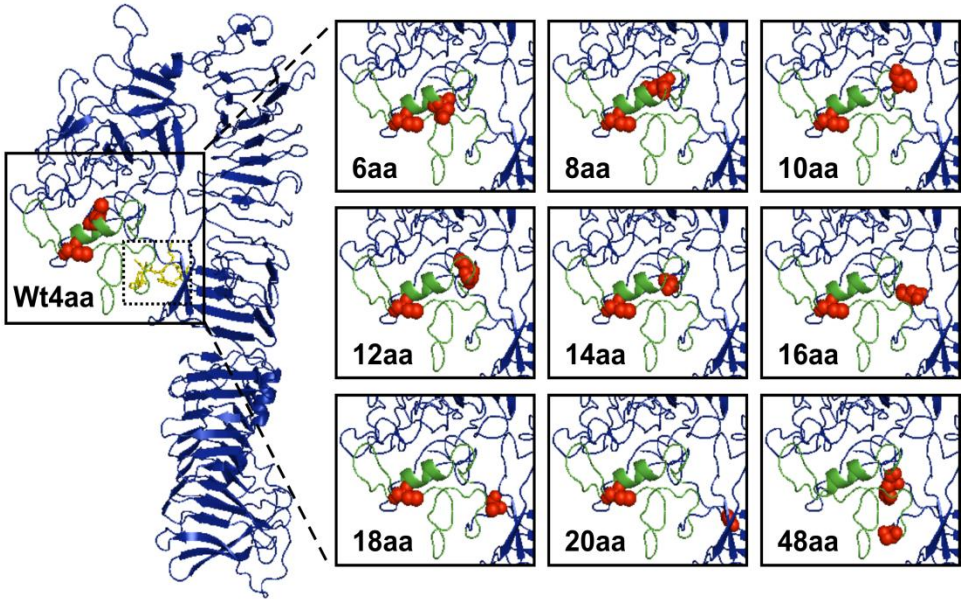

**Fig. S3**

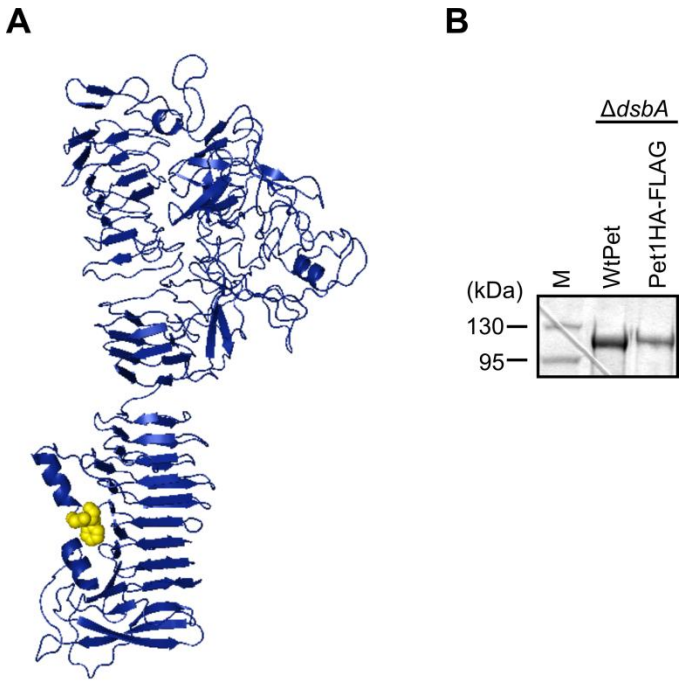

# Fig. S4

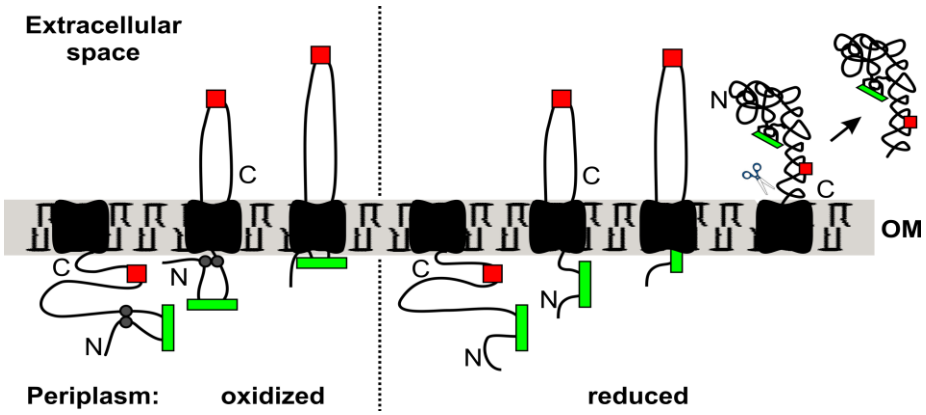
Extracellular space
C
C
N
C
N
C
C
N
N
N
C
OM
Periplasm:
oxidized
reduced

# Size and Conformation Limits to Secretion of Disulfide-bonded Loops in Autotransporter Proteins

Denisse L. Leyton, Yanina R. Sevastsyanovich, Douglas F. Browning, Amanda E. Rossiter, Timothy J. Wells, Rebecca E. Fitzpatrick, Michael Overduin, Adam F. Cunningham and Ian R. Henderson

*J. Biol. Chem. 2011, 286:42283-42291.*
*doi: 10.1074/jbc.M111.306118 originally published online October 17, 2011*

---